Available online at www.sciencedirect.com
ScienceDirect
International Journal of Mass Spectrometry 267 (2007) 338–345
International Journal of Mass Spectrometry
www.elsevier.com/locate/ijms

Strong and very strong hydrogen bonding in fluoro-amine–fluoride systems

R.J. Nieckarz *, N. Oldridge, T.B. McMahon *

Department of Chemistry, University of Waterloo, Waterloo, Ontario N2L 3G1, Canada

Received 8 November 2006; received in revised form 22 March 2007; accepted 26 March 2007
Available online 30 March 2007

Dedicated to the memory of Sharon Lias whose efforts in Gaseous Ion Thermochemistry are greatly appreciated and sadly missed.

Abstract

The formation of strong and very strong hydrogen bonds between NF_nH_{3-n} ($n = 0.2$) and F^- have been computationally investigated via B3LYP/6-311++G(d,p) geometry optimizations and MP2/6-311++G(d,p) single point energy calculations. The enthalpy of deprotonation of NF_2H was found to be 1518.5 kJ mol^{-1}. The hydrogen bond energy in $NH_3\cdots F^-$, $NFH_2\cdots F^-$ and $NF_2H\cdots F^-$ were calculated to be 67.9, 120.2 and 181.2 kJ mol^{-1}, respectively, and clearly show the effect of fluorination on hydrogen bond strength in amine–fluoride systems. The change in enthalpy and entropy for the clustering of methanol to $NF_2H\cdots F^-$ to form the fluoride bound dimer of methanol and difluoramine has been measured via high pressure mass spectrometry to be 68.3 kJ mol^{-1} and 90.5 J K^{-1} mol^{-1}. These values are in excellent agreement with calculated values of 70.9 kJ mol^{-1} and 88.5 J K^{-1} mol^{-1}.

Keywords: Hydrogen bonding; Fluoride; Fluoro-amine; Thermochemistry; High pressure mass spectrometry

1. Introduction

In the solid and liquid phases, NF_2H (difluoramine) has attracted considerable attention based on its highly unstable and explosive nature [1–3]. The extremely volatile nature of this compound makes it very dangerous to work with and significant safety precautions must be taken when dealing with it. In the gas-phase, difluoramine is much safer to handle and, as such, it has been possible for it to be characterized by IR, microwave and UV spectroscopy [4–6]. Despite the considerable interest in the condensed phase of difluoramine as a potential explosive and fuel [7], relatively few gas-phase investigations of clusters of difluoramine have been performed [8,9] as a source of insight into the true nature of the intermolecular interactions intrinsic to this molecule.

The presence of the both the NH moiety and lone pairs of electrons on nitrogen and fluorine in difluoramine make it an appealing candidate for hydrogen bond formation. In addition, Yamdagni and Kebarle first demonstrated that hydrogen bond strength, $D(BH\cdots X^-)$, will increase both with the acidity of an acid, BH, and the basicity of an ionic base, X^- [10]. It has also previously been demonstrated that fluorination of an acid, BH, can lead to both an increase in the gas-phase acidity of BH and a stronger $BH\cdots X^-$ hydrogen bond. This is demonstrated, for example, by the hydrogen bonding properties of ethanol and 1,1,1 trifluoroethanol. The substitution of fluorine in ethanol to form CF_3CH_2OH results in a decrease in the enthalpy of deprotonation from 1586.2 kJ mol^{-1} [11] to 1513 kJ mol^{-1} [12], indicating a substantial increase in the gas-phase acidity. When CH_3CH_2OH and CF_3CH_2OH are clustered with the anionic base F^-, the measured OHF hydrogen bond strengths are −135.6 kJ mol^{-1} [13] and −164 kJ mol^{-1} [14], respectively. The difference in values of ΔH^0_{rxn} for the deprotonation of NF_2H and NH_3 are even greater and reported in the literature as −1552 kJ mol^{-1} [15] and −1563 kJ mol^{-1} [16] for NF_2H and −1687.8 kJ mol^{-1} [17] for NH_3. Based on these arguments, difluoramine would be expected to participate in stronger hydrogen bonds with F^- than would NH_3 and is a very likely candidate to form very strong hydrogen bonds.

The present study involves an investigation of difluoramine in hydrogen bonding environments from both experimental and computational perspectives. Using high pressure mass spectrometry (HPMS), thermochemical properties associated with

* Corresponding author. Tel.: +1 519 888 4591; fax: +1 519 746 0435.
E-mail addresses: rnieckar@uwaterloo.ca (R.J. Nieckarz), toldridg@sciborg.uwaterloo.ca (N. Oldridge), mcmahon@uwaterloo.ca (T.B. McMahon).

1387-3806/$ – see front matter © 2007 Published by Elsevier B.V.
doi:10.1016/j.ijms.2007.03.016

difluoramine have been measured. This technique allows for the creation of ions derived from potentially dangerous compounds in situ, greatly increasing the safety of the experiment. Also, computational investigations of difluoramine as well as clusters of interest, specifically that shown in Eq. (1), have been performed to help further develop the understanding of very strong hydrogen bonds which can form in these amine–fluorine systems.

$$NF_2H\cdots F^- + CH_3OH \overset{K_{eq}}{\rightleftharpoons} NF_2H\cdots F^-\cdots CH_3OH \quad (1)$$

2. Experimental

All experimental measurements were conducted using a high-pressure mass spectrometer configured around a VG 8-80 magnetic sector mass spectrometer. A detailed description of this instrument has been given elsewhere [18].

In a heated 5 L reservoir, a known amount (between 2 and 40 μL) of CH_3OH was injected into a mixture containing 9 Torr NF_3 in 900 torr CH_4·CH_3OH (99.8% purity), NF_3, and CH_4 (99.97% purity) were purchased from Sigma–Aldrich, Ozark Mahoning, and Praxair, respectively. Chemicals were used as supplied with no further purification performed. This mixture was introduced into the ion source at a constant total pressure and, using 2 keV electron pulses of 60 μs duration with a repetition period of 60 ms, small, but reproducible ionic signals corresponding to $NF_2H\cdots F^-$ and $NF_2H\cdots F^-\cdots CH_3OH$ were observed.

There are several different possible explanations for the presence of the difluoramine containing species within the ion source. One possibility is that a small amount of NF_2H is present as a contaminant in the commercial sample of NF_3. Gaseous NF_2H is known to react with metal surfaces to decompose into HF and tetrafluorohydrazine [2,3,19] and it is possible that tetraflurohydrazine itself may react subsequently with protic species to regenerate NF_2H. A second possibility is the direct synthesis of NF_2H within the ion source, initiated by ionization of the gas mixture. Slow secondary electrons or low energy electrons resulting from the thermalization of the 2 kV electrons entering the source, can undergo dissociative electron capture to NF_3, Eq. (2) [16] and the resulting $NF_2^\bullet$ species can then react with CH_4 to generate NF_2H, Eq. (3).

$$NF_3 + e^- \rightarrow F^- + NF_2^\bullet \quad (2)$$

$$NF_2^\bullet + CH_4 \rightarrow NF_2H + CH_3 \quad (3)$$

Whatever the mechanism of formation, once NF_2H and $NF_2H\cdots F^-$ are present in the ion source they may readily associate with fluoride and methanol, respectively, leading to the formation of the fluoride bound dimer of difluoramine and methanol, Eqs. (4) and (5).

$$F^- + NF_2H \rightarrow NF_2H\cdots F^- \quad (4)$$

$$NF_2H\cdots F^- + CH_3OH \overset{K_{eq}}{\rightleftharpoons} NF_2H\cdots F^-\cdots CH_3OH \quad (5)$$

All ions are generated in the electric field free ion source in the presence of a bath gas, in this case CH_4, and, at the experimental pressures used, newly formed ions will have undergone approximately 10^8 collisions before diffusing out of the ion source.[1] This ensures that all ions attain thermal equilibrium within the residence time in the ion source.

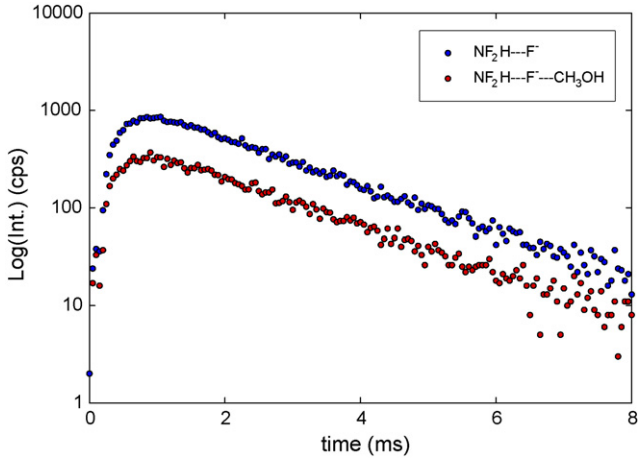

Fig. 1. Time-intensity profiles for $NF_2H\cdots F^-$ and $NF_2H\cdots F^-\cdots CH_3OH$ at 117 °C and P_{CH_3OH} = 7.45 millitorr. Each profile is the result of the summation of ion intensity after 7000 electron gun pulses.

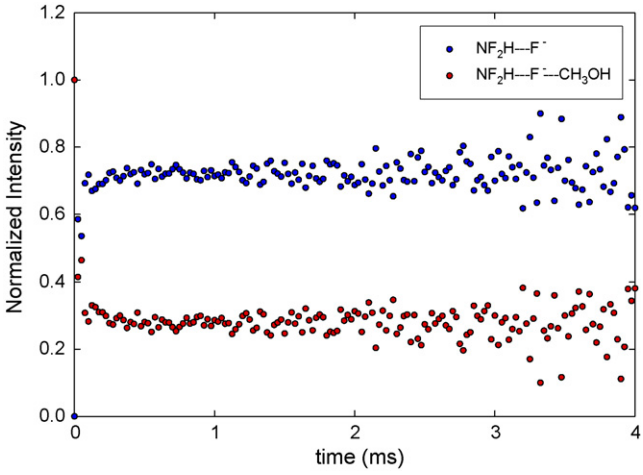

Fig. 2. Normalized time-intensity profiles for $NF_2H\cdots F^-$ and $NF_2H\cdots F^-\cdots CH_3OH$. Equilibrium is established 0.5 ms after ionization and lasts until 3 ms after ionization. The apparent divergence observed after 4 ms is an artifact of low signal intensity and is not an indication that the system is not at equilibrium.

Using an EG&G Ortec multichannel scalar data acquisition system, 7000 accumulations of ion intensity as a function of time after ionization were summed for all ionic species in reaction (1). This large number of accumulations was necessary to improve the signal to noise ratio of the low intensity ion signals involved. Typical time-intensity and normalized time intensity plots can be found in Figs. 1 and 2, respectively. Normalization of the two resulting time–intensity profiles with respect to each other allowed for the identification of the presence of thermal equilibrium 0.5 ms after the end of the electron gun pulse as indicated by the parallel horizontal region in Fig. 1.

[1] Estimated using the Langevin Equation for collisional rate constants.

A functional form of the equilibrium constant associated with reaction (1), which allows for the determination of various thermochemical properties, is given by Eq. (6).

$$K_{eq} = \frac{I_{[NF_2H\cdots F\cdots CH_3OH]^-}}{I_{[NF_2H\cdots F]^-} P_{[CH_3OH]}} P_o \quad (6)$$

From the ratio of ion intensities during the period of time in which the two species are in equilibrium, the known partial pressure of the neutral gas and the reference pressure of $P_o = 1$ bar, K_{eq} is obtained. If measurements of K_{eq} are carried out over a temperature range in which no significant isomerization or changes in heat capacity occur, values for ΔH^0_{rxn} and ΔS^0_{rxn} can be obtained from a plot of $\ln(K_{eq})$ as a function of $1/T$. The resulting van't Hoff equation, Eq. (7), predicts a straight line with a slope of

$$\ln K_{eq} = -\frac{\Delta H^0_{rxn}}{RT} + \frac{\Delta S^0_{rxn}}{R} \quad (7)$$

$-\Delta H^0_{rxn}/R$ and an intercept equal to $\Delta S^0_{rxn}/R$. All temperature measurements were made using a J-type thermocouple (accuracy of ±1 K) placed in direct contact with the walls of the ion source. Absolute errors in ΔH^0_{rxn} and ΔS^0_{rxn} are based upon propagation of uncertainties in pressure and temperature and taken as ±2 kJ mol^{-1} and ±10 J mol^{-1} K^{-1}, respectively.

As a complement to experiments, a combination of DFT and ab initio calculations was performed on a number of species relevant to this study. These calculations were carried out using the commercially available Gaussian 03 software [20] while images of optimized ions and molecules were obtained from the GaussView 3.0 program [21]. Geometry optimizations and frequency calculations were performed using the B3LYP level of theory with a 6-311++G(d,p) basis set with no scaling of frequencies. The electronic energy of each optimized structure was then calculated via an MP2(full) single point calculation, also employing the 6-311++G(d,p) basis set. This compound method takes advantage of both the speed of B3LYP methods and their associated ability to accurately reproduce structural details, while at the same time achieving the higher energy accuracy from the fully correlated MP2 calculation [22].

ΔH^0_{rxn} and ΔS^0_{rxn} for reaction (1) were obtained by performing geometry optimizations, frequency calculations and single point calculations on all species involved and taking the appropriate differences between products and reactants. In the case of the enthalpy change, Eq. (8),

$$\Delta H^0_{rxn} = \Delta E^{elec} + \Delta ZPE + \Delta E^{vib} + \Delta E^{rot} + \Delta E^{trans} + w, \quad (8)$$

ΔE^{elec} is the difference in electronic energy between products and reactants, ΔZPE is the difference in zero point energies, ΔE^{vib}, ΔE^{rot} and ΔE^{trans} are the differences of vibrational, rotational and translational energies, respectively, and w is the pressure–volume work done in going from two moles of reactant gas to one mole of product gas. For (1), $w = -RT$. In the case of entropy change, Eq. (9)

$$\Delta S^0_{rxn} = \sum_{products} S^0_i - \sum_{reactants} S^0_j, \quad (9)$$

$\sum_{products} S^0_i$ and $\sum_{reactants} S^0_j$ represent the sums of translational, electronic, vibrational and rotational entropies over all product and reactant species, respectively.

3. Results and discussion

3.1. Thermochemical data

The van't Hoff plot shown in Fig. 3 for reaction (1) was obtained over a 92 °C temperature range from 55 to 147 °C. From this plot, ΔH^0_{rxn} and ΔS^0_{rxn} for reaction (1) were found to be -68.3 ± 2 kJ mol^{-1} and -90.5 ± 10 J mol^{-1} K^{-1}, respectively. An expected increase in the scatter of data points in Fig. 3 was present due to the extremely low signal intensities that were observed for this system, yet excellent linearity remained over the entire temperature range.

The minimum energy structures for $NF_2H\cdots F^-$, CH_3OH and $NF_2H\cdots F^-\cdots CH_3OH$ obtained from B3LYP/6-311++G(d,p) optimizations are shown in Fig. 4 as II, III, and V, respectively. The calculated values of ΔH^0_{rxn} and ΔS^0_{rxn} for reaction (1) based on these optimized structures were -70.9 kJ mol^{-1} and -88.5 J mol^{-1} K^{-1}, respectively, and are in excellent agreement with the experimentally obtained values reported above. A more detailed discussion of all structures found in Fig. 4 is given below.

Two different routes for the formation of $NF_2H\cdots F^-\cdots CH_3OH$ clusters from NF_2H, CH_3OH, and F^-, as shown in Fig. 5, can be envisioned. The enthalpy change for reaction (1) measured in the present study corresponds to the second step involved in Path 2. In order for this route to be followed, as a first step, a very strong hydrogen bond must be formed between NF_2H and F^-. The enthalpy change for this

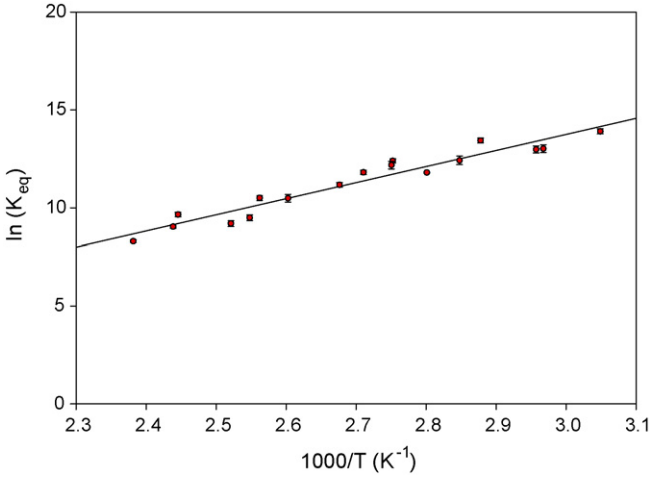

Fig. 3. van't Hoff plot collected over a 92 °C temperature range from 55 to 147 °C for clustering of $NF_2H\cdots F^-$ with CH_3OH. Error bars on each data point indicate standard deviation of 6–10 repetitive measurements of K_{eq} at each temperature.

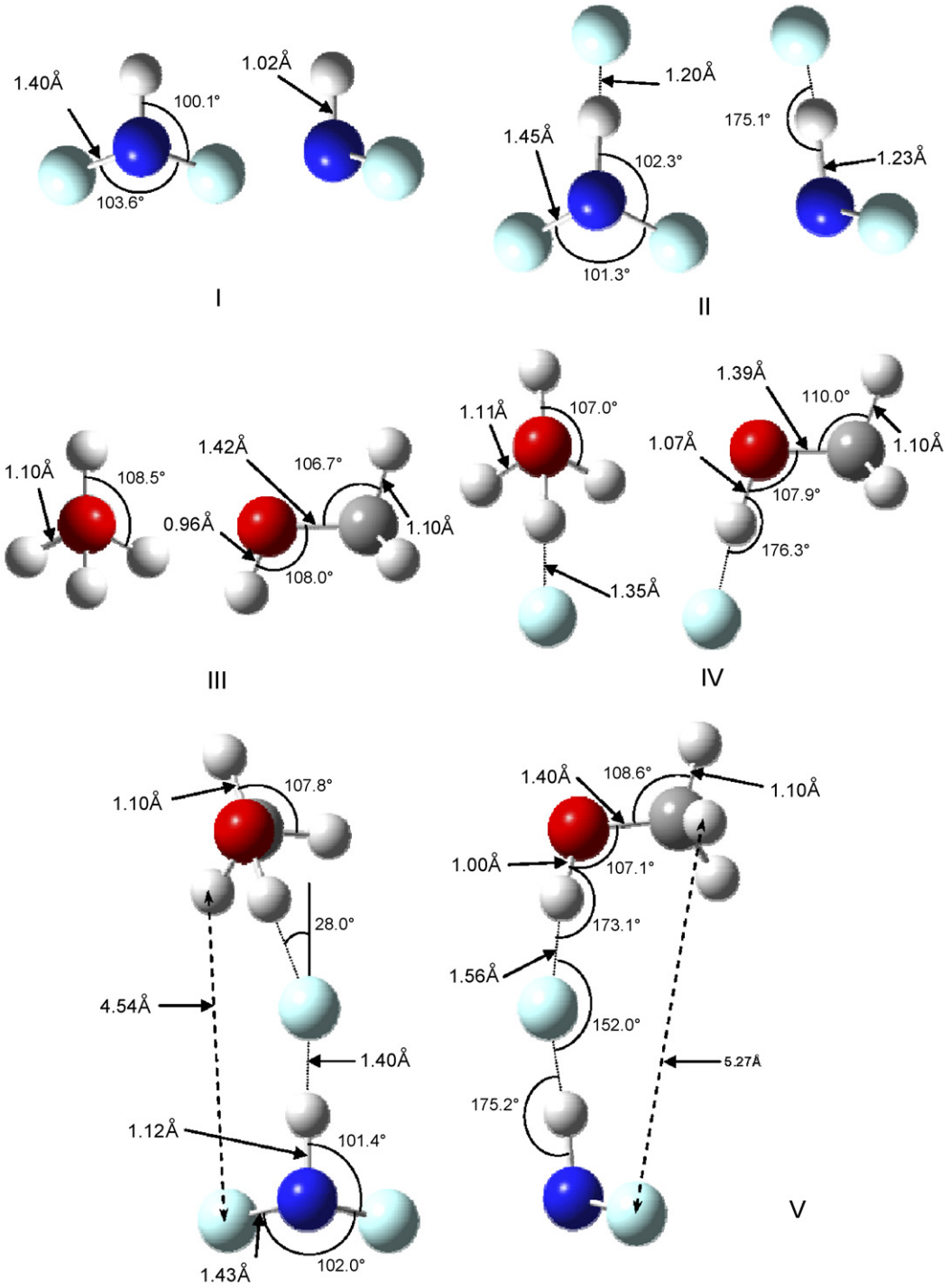

Fig. 4. Optimized geometries obtained from B3LYP/6-311++G(d,p) calculations: (I) NF_2H; (II) $NF_2H\cdots F^-$; (III) CH_3OH; (IV) $CH_3OH\cdots F^-$; (V) Fluoride bound dimer of CH_3OH and NF_2H. All distances are in Å and bond angles are in degrees.

bond formation reaction was calculated to be $-181.2\,kJ\,mol^{-1}$, which, in terms of bond strength, comes close to equaling the very strong hydrogen bond strength present in FHF^- ($\Delta H^0_{rxn} = -192\,kJ\,mol^{-1}$)[23]. Path 1 in Fig. 5 outlines an alternative route for the formation of the fluoride bound clusters of methanol and difluoramine. The initial step in Path 1 involves the addition of methanol to fluoride, which has been previously examined by DeTuri and Ervin using TCID [11] and by Larson and McMahon employing ion molecule reaction equilibria in an FT-ICR [14]. DeTuri and Ervin found ΔH^0_{rxn} to be $-123 \pm 9.2\,kJ\,mol^{-1}$, while Larson and McMahon obtained ΔH^0_{rxn} to be $-124 \pm 8.4\,kJ\,mol^{-1}$. Both of these measurements are consistent with the value of $-129\,kJ\,mol^{-1}$ computed in this study. Larson and McMahon [14] also report a ΔS^0_{rxn} for this step of $-94.6\,J\,mol^{-1}\,K^{-1}$, which is in excellent agreement with the calculated value of $-95.7\,J\,mol^{-1}\,K^{-1}$.

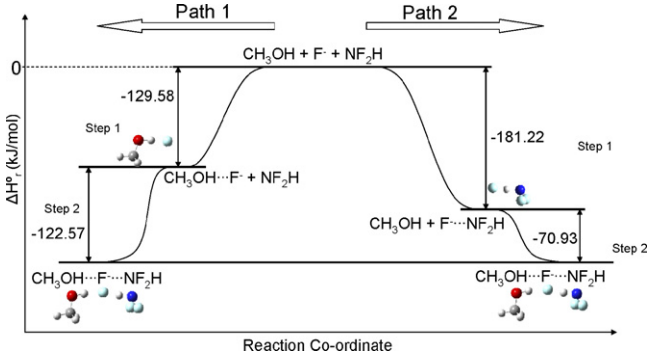

Fig. 5. Calculated reaction profile for the formation of $CH_3OH\cdots F^-\cdots NF_2H$ clusters using B3LYP/6-311++G(d,p). Two pathways, each consisting of two steps, are shown.

Table 2
Calculated and literature values of ΔH^0_{rxn}(kJ mol^{-1}) for $NF_nH_{3-n} \rightleftarrows NF_nH_{2-n}^- + H^+$ using B3LYP/6-311++G(d,p) optimized geometry and MP2(full)/6-311++G(d,p) electronic energy

Reaction	Calculated (kJ/mol)	Literature (kJ/mol)
$NH_3 \rightleftarrows NH_2^- + H^+$	−1695.2	−1687.8[a]
$NFH_2 \rightleftarrows NFH^- + H^+$	−1614.4	–
$NF_2H \rightleftarrows NF_2^- + H^+$	−1518.5	−1552[b] −1563[c] −1506[d]

[a] Ref. [17].
[b] Ref. [15].
[c] Ref. [16].
[d] Ref. [27]. Estimated using $\Delta G^0_{rxn} + T\Delta S^0_{rxn}$, where $T\Delta S^0_{rxn} = 29$ kJ/mol.

Calculations were also performed in order to gain further insight into the effect of fluorine substitution in ammonia-fluoride hydrogen bonded systems by examining the formation equilibria of $NF_nH_{3-n}\cdots F^-$ ($n = 0,\ldots,2$) clusters. The optimized geometries of these clusters are shown in Fig. 6 and the thermochemical data for the cluster formation is given in Table 1. A detailed discussion of the structural aspects of the clusters shown in Fig. 6 is given below. A plot of the fluoride binding enthalpy, ΔH^0_{FBE}, versus gas phase acidity, ΔH^0_{acid}, for the $NF_nH_{3-n}\cdots F^-$ system is shown in Fig. 7. The expected linear relationship between gas phase acidity and fluoride binding enthalpy was observed. Each sequential fluorine substitution for hydrogen in NH_3 increases the strength of the $NH\cdots F^-$ hydrogen bond by approximately 60 kJ mol^{-1}. Calculated and, where available, experimental literature values for the enthalpy of deprotonation of NH_3, NFH_2 and NF_2H are reported in Table 2. The expected increase in gas-phase acidity as a function of fluorination was observed, and in the case of NH_3 good agreement between literature and calculated values can be seen. There is currently no reference value available for NFH_2, while a large uncertainty in the value for NF_2H exists. Three different values for the acidity of NF_2H are reported in the literature, spanning more than a 50 kJ/mol range. It is believed that the stronger, calculated gas-phase acidity reported in this work better represents the actual acidity of NF_2H. This conclusion is based on the excellent agreement of the measured thermochemical data for the NF_2H clusters reported above and a comparison to other simple hydrogen bond forming systems.

The calculation method and level of theory employed here have been shown by others to be very successful in accurately replicating geometries of hydrogen bonding systems [22] and, as such, should prove to be a reliable method for predicting properties of the nitrogen–hydrogen, oxygen–hydrogen, and fluorine–hydrogen bonding clusters studied. As a test, the enthalpy of deprotonation of HF, CH_3OH, and NH_3, as well as the fluoride affinities of HF, CH_3OH, and H_2O were calculated using various basis sets. It was confirmed that the combination of B3LYP/6-311++G(d,p) optimizations with MP2(full)/6-311++G(d,p) single point electronic energy calculations provided the best agreement for all test cases, giving an agreement with literature values better than or equal to 8 kJ mol^{-1}, and in many cases much better. The excellent agreement between calculated and experimental thermochemical data reported in this study thus increases the confidence in the ability of this calculation method to accurately describe these systems.

For AXH acids of the same gas-phase acidity, where X = N, O, or F, it has been shown that upon the formation of hydrogen bonds to an anionic base, B^-, $AXH\cdots B^-$ hydrogen bond strength increases when X is changed from N to O to F. A comparison of the deprotonation and fluoride binding energies of HF, CFH_2CH_2OH and NF_2H provides insight into what the relative magnitudes of each of these should be. In the case of HF, the enthalpy of deprotonation is 1554 kJ mol^{-1} [24], while its

Table 1
Summary of thermodynamic data pertaining to equilibrium reactions studied

Reaction	ΔH^0_{rxn} kJ mol^{-1}	ΔS^0_{rxn} J mol^{-1} K^{-1}	Method/ reference
$NF_2H\cdots F^- + CH_3OH \rightleftarrows NF_2H\cdots F^-\cdots CH_3OH$	−68.3	−90.5	a/d
	−70.9	−88.5	b/d
$CH_3OH\cdots F^- + NF_2H \rightleftarrows NF_2H\cdots F^-\cdots CH_3OH$	−122.6	−95.8	b/d
$CH_3OH\cdots F^- \rightleftarrows CH_3OH\cdots F^-$	−129.6	−95.7	b/d
	−124	−94.6	c/e
$NF_2H + F^- \rightleftarrows NF_2H\cdots F^-$	−181.2	−102.9	b/d
$NFH_2 + F^- \rightleftarrows NFH_2\cdots F^-$	−120.2	−98.9	b/d
$NH_3 + F^- \rightleftarrows NH_3\cdots F^-$	−67.9	−85.1	b/d

a: HPMS, b: MP2(full)/6-31 l++G(d,p)//B3LYP/6-311++G(d,p), c: ion molecule reaction equilibrium, d: this study, e: Larson and McMahon [14].

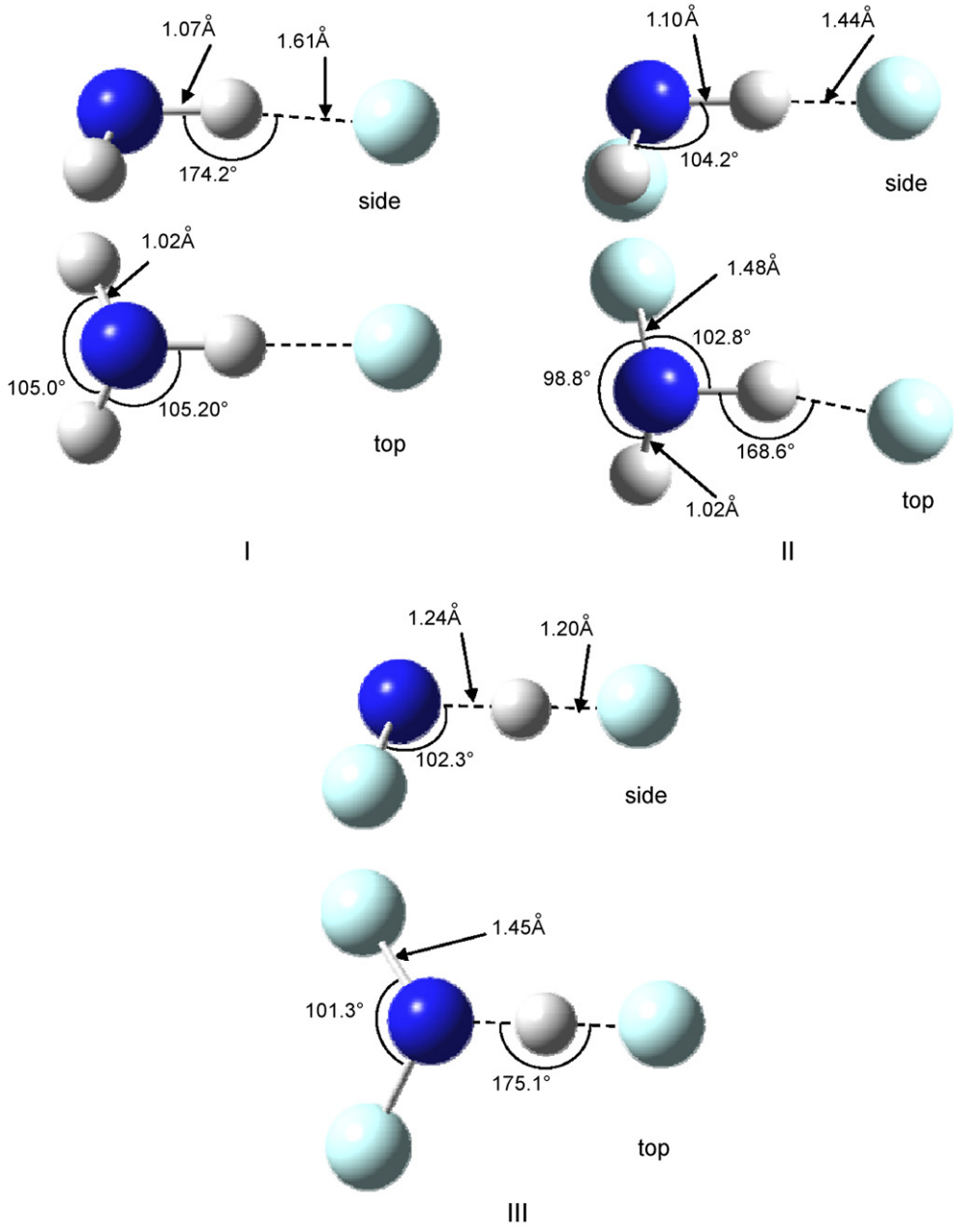

Fig. 6. Optimized geometries obtained from B3LYP/6-311++G(d,p) calculations: (I) $NH_3\cdots F^-$ (II) $NFH_2\cdots F^-$ (III) $NF_2H\cdots F^-$.

binding energy to F^- is 192 kJ mol^{-1} [23]. In the case of the 2-fluoroethanol the enthalpy of deprotonation is 1553 kJ mol^{-1} [25], while its binding energy to F^- is 146 kJ mol^{-1} [14], an observable decrease in fluoride binding energy of nearly 50 kJ mol^{-1}. If the gas-phase acidity of NF_2H was closer to the literature value of 1552 kJ mol^{-1} the expected fluoride binding energy of NF_2H would be well below that of 2-fluoroethanol, yet calculations predict a significantly larger value of 181 kJ mol^{-1}. In order to explain the unexpectedly large fluoride binding energy of NF_2H an increase in its gas-phase acidity would thus be anticipated, as predicted by calculations.

The ability of difluoramine to form very strong hydrogen bonds was essential in permitting this system to be studied. In order to measure equilibrium constants in an HPMS experiment a ratio of ion intensities less than 100 is desirable. Since only very small amounts of NF_2H were present in the ion source, it was necessary to introduce only very small amounts of methanol. In the absence of the very strong hydrogen bond found in $NF_2H\cdots F^-$, it would not have been possible to generate this species and thus to perform these experiments.

3.2. Structural aspects of $NF_2H\cdots F^-\cdots CH_3OH$ and $NF_nH_{3-n}\cdots F^-$ (n = 0,. . .,2) cluster formation

3.2.1. $NF_nH_{3-n}\cdots F^-$ (n = 0,. . .,2) clusters

In the case of the sequentially fluorinated ammonia–fluoride clusters, interesting observations regarding the connection between NHF bond geometry and bond strength can be made.

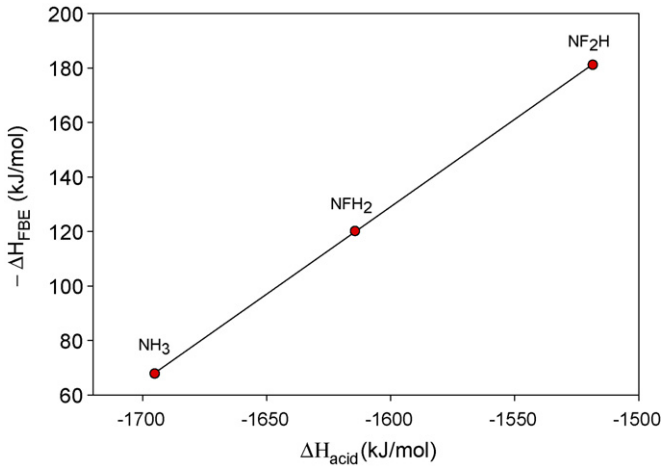

Fig. 7. Plot of fluoride binding enthalpy (ΔH_{FBE}) versus gas phase acidity (ΔH_{acid}) demonstrates the effect of fluorine substitution on hydrogen bond strength in the $NF_nH_{3-n}\cdots F^-$ system. Electronic energies//optimized geometries obtained from MP2(full)/6-31 l++G(d,p)//B3LYP/6-311++G(d,p) calculations.

The $NH_3\cdots F^-$ cluster depicted in Fig. 6I reveals that the formation of a N–H–F hydrogen bond of $-67.9\,kJ\,mol^{-1}$ is accompanied by an increase in the NH bond length from 1.01 Å in NH_3 (calculated in this study) to 1.07 Å in the cluster.

The mono-substitution of fluorine for hydrogen in ammonia to form NFH_2 (Fig. 6II) initiates changes in the geometry and physical properties of the species. The root of most of these changes is the electron withdrawing effect of fluorine which causes an increase in the gas-phase acidity of the species, an increase in the NH bond polarity and a stronger hydrogen bond ($-120.2\,kJ\,mol^{-1}$) in the cluster with fluoride ion. A slightly larger shift in NH bond length from 1.02 Å in NFH_2 to 1.10 Å in $NFH_2\cdots F^-$ can be seen when the hydrogen bond is formed, also indicating a stronger hydrogen bond relative to that in $NH_3\cdots F^-$.

The difluoro-substitution of ammonia to form NF_2H further amplifies the changes noted in the mono-fluorinated case. An additional increase in gas-phase acidity, bond polarity and hydrogen bond strength ($-181.2\,kJ\,mol^{-1}$) can all be noted, as well as the increase in NH bond distance upon clustering with fluoride from 1.03 Å in NF_2H to 1.20 Å in $NF_2H\cdots F^-$.

The NH bond distance and total NHF bond distance across the $NF_nH_{3-n}\cdots F^-$ system in order of increasing fluorination (i.e. NH_3 to NFH_2 to NF_2H) are 1.07, 1.10, and 1.20 and 2.67, 2.54, and 2.44 Å, respectively. This decrease in total bond distance and hydrogen shift away from the nitrogen are strongly indicative of the increasing hydrogen bond strength and increased gas-phase acidity of the fluoro-amine species. It is interesting to note that in the case of the NF_2H fluoride adduct the proton is very close to being equally shared between N and F. This further supports the idea that the acidity of NF_2H is greater than that of HF since nitrogen acids are expected to bond more weakly than HF if they have comparable gas phase acidities.

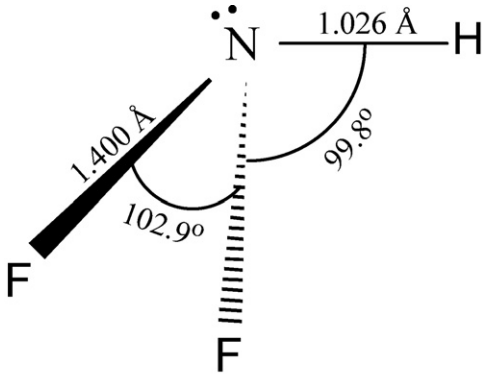

Fig. 8. Structure of NF_2H as determined from microwave spectroscopy by Lide [5].

3.2.2. $NF_2H\cdots F^-\cdots CH_3OH$ clusters

The geometry of neutral difluoramine calculated in this study and shown in Fig. 4I is in excellent agreement with the structure obtained from microwave spectroscopy reported in Fig. 8. This structure is also consistent with the structure of difluoramine determined computationally by Demaison and co-workers using the same level of theory and basis set as that used in this study [26]. An examination of changes in geometry in proceeding from structures I–II–V and III–IV–V, as well as using the changes in enthalpy reported in the two pathways of Fig. 5, permits a better understanding of this hydrogen bond system.

Path 1 in Fig. 5 represents the initial clustering of methanol to fluoride, followed by the clustering of $CH_3OH\cdots F^-$ with difluoramine. The structures involved in this process are shown in Fig. 4 as III, IV and V. The initial clustering of methanol to fluoride results in a strong hydrogen bond between the hydroxyl hydrogen of methanol and F^- ($\Delta H^0_{rxn} = -129.6\,kJ\,mol^{-1}$) and results in an increase in O–H bond length from 0.96 to 1.07 Å, and a total O–F bond distance of 2.42 Å. The subsequent clustering with difluoramine reduces the strength of interaction between the fluoride and the hydroxyl group, resulting in a decrease in O–H bond length to 1.00 Å. This decreased $OH\cdots F$ hydrogen bond strength in the di-solvated fluoride cluster is also manifested in the increased total O–F bond distance of 2.56 Å.

Path 2 in Fig. 5 represents the initial clustering of difluoramine with fluoride to form a very strong $NH\cdots F$ hydrogen bond ($\Delta H^0_{rxn} = -181.2\,kJ\,mol^{-1}$), followed by the clustering with methanol to form the mixed fluoride bound dimer. The very much stronger interaction of fluoride with NF_2H relative to that with methanol is an indicator of the surprising and substantial acidity of NF_2H. The initial formation of the $NH\cdots F$ bond results in an increase in NH bond length from 1.02 to 1.23 Å and a total N–F bond length of 2.43 Å. Although the N–F bond length in II is almost identical to the O–F bond length in IV, one notable difference is that the $NH\cdots F$ hydrogen bond possesses a near symmetric sharing of the proton. This once again indicates that the gas-phase acidity of NF_2H is comparable in magnitude to the acidity of HF, but also implies that it is substantially greater than that of CH_3OH. This greater acidity is also evident from the very significant decrease in the strength of interaction of CH_3OH with $NF_2H\cdots F^-$. In contrast, the strengths of interac-

tion in the two steps in Path 1 were comparable. A decrease in N–H bond distance to 1.12 Å, an increase in F–H bond distance to 1.40 Å and an increase in N–F bond distance to 2.52 Å are also seen.

4. Conclusion

The mixed fluoride bound cluster of difluoramine and methanol provides a wealth of information concerning strong and very strong hydrogen bonds. The effect of fluorine substitution on $NF_nH_{3-n}\cdots F^-$ systems is quite evident as demonstrated by the monotonic increase in hydrogen bond strength in the order $NH_3\cdots F^- < NFH_2\cdots F^- < NF_2H\cdots F^-$. The enthalpy of deprotonation of NF_2H was found to be 1518.5 kJ mol^{-1}. The predicted changes in enthalpy observed in the two pathways for the formation of the fluoride bound clusters of methanol and difluoramine are consistent with the geometric changes obtained from calculated structures. Further experiment to measure ΔH^0_{rxn} and ΔS^0_{rxn} of formation for clusters of the type $NF_nH_{3-n}\cdots F^-$ ($n = 0.2$) or the addition of NF_2H to $CH_3OH\cdots F^-$ would definitely be useful to confirm the predictions of the calculations performed in this study.

Acknowledgements

The financial support of the Natural Sciences and Engineering Research Council of Canada in the form of a Discovery Grant to TBM and an Undergraduate Student Research Assistantship to N.O. is gratefully acknowledged, as is the scholarship support to R.N. by the Ontario Graduate Scholarship fund.

References

[1] E.A. Lawton, J.Q. Weber, J. Am. Chem. Soc. 81 (1959) 4755.
[2] C.J. Hoffman, R.G. Neville, Chem. Rev. 62 (1962) 1.
[3] E.A. Lawton, J.Q. Weber, J. Am. Chem. Soc. 85 (1963) 3595.
[4] J.J. Comeford, D.E. Mann, L.J. Schoen, D.R. Lide Jr., J. Chem. Phys. 38 (1963) 461.
[5] D.R. Lide Jr., J. Phys. Chem. 38 (1963) 456.
[6] D. Colbourne, D.C. Frost, C.A. McDowell, N.P.C. Westwood, Chem. Phys. Lett. 72 (1980) 247.
[7] P. Politzer, P. Lane, M.E. Grice, M.C. Concha, P.C. Redfern, J. Mol. Struct. (Theochem) 338 (1995) 249.
[8] X.-H. Ju, H.-M. Xiao, Propell. Explos. Pyrotech. 27 (2002) 320.
[9] M. Solimannejad, A. Boutalib, J. Chem. Phys. A 108 (2004) 10342.
[10] R. Yamdagni, P. Kebarle, J. Am. Chem. Soc. 93 (1971) 7139.
[11] V.F. DeTuri, K.M. Ervin, J. Phys. Chem. A 103 (1999) 6911.
[12] J.E. Bartmess, J.A. Scott, R.T. Mclver Jr., J. Am. Chem. Soc. 101 (1979) 6046.
[13] B. Bogdanov, M. Peschke, D.S. Tonner, J.E. Szulejko, T.B. McMahon, Int. J. Mass Spectrom. 185–187 (1999) 707.
[14] J.W. Larson, T.B. McMahon, J. Am. Chem. Soc. 105 (1983) 2944.
[15] L.A. Koppel, R.W. Taft, F. Anvia, S.-Z. Zhu, L.-Q. Hu, K.-S. Sung, D.D. DesMarteau, L.M. Yagupolskii, Y.L. Yagupolskii, N.V. Ignat'ev, N.V. Kondratenko, A.Y. Volkonskii, V.M. Vlasov, R. Notario, P.-C. Maria, J. Am. Chem. Soc. 116 (1994) 3047.
[16] N. Ruckhaberle, L. Lehmann, S. Matejcik, E. Illenberger, Y. Bouteiller, V. Periquet, L. Museur, C. Desfrancois, J.-P. Schermann, J. Phys. Chem. A 101 (1997) 9942.
[17] C.T. Wickham-Jones, K.M. Ervin, G.B. Ellison, W.C. Lineberger, J. Chem. Phys. 91 (1989) 2762.
[18] J.E. Szulejko, J.J. Fisher, T.B. McMahon, J. Wronka, J. Mass Spectrom. Ion Process. 83 (1988) 147.
[19] J.C. Oxley, J.L. Smith, J. Zhang, C. Bedford, J. Phys. Chem. A 105 (2001) 579.
[20] M.J. Frisch, G.W. Trucks, H.B. Schlegel, G.E. Scuseria, M.A. Robb, J.R. Cheeseman, J. Montgomery, J.A.T. Vreven, K.N. Kudin, J.C. Burant, J.M. Millam, S.S. Iyengar, J. Tomasi, V. Barone, B. Mennucci, M. Cossi, G. Scalmani, N. Rega, G.A. Petersson, H. Nakatsuji, M.E. Hada, M.K. Toyota, R. Fukuda, J. Hasegawa, M. Ishida, T. Nakajima, Y. Honda, O. Kitao, H. Nakai, M. Klene, X. Li, J.E. Knox, H.P. Hratchian, J.B. Cross, V. Bakken, C. Adamo, J. Jaramillo, R. Gomperts, R.E. Stratmann, O. Yazyev, A.J. Austin, R. Cammi, C. Pomelli, J.W. Ochterski, P.Y. Ayala, K. Morokuma, G.A.S. Voth, P.J.J. Dannenberg, V.G. Zakrzewski, S. Dapprich, A.D.S. Daniels, M.C.O. Farkas, D.K. Malick, A.D. Rabuck, K. Raghavachari, J.B. Foresman, J.V. Ortiz, Q. Cui, A.G. Baboul, S. Clifford, J. Cioslowski, B.B. Stefanov, G. Liu, A. Liashenko, P. Piskorz, I.M. Komaromi, R.L.D.J. Fox, T. Keith, M.A. Al-Laham, C.Y. Peng, A. Nanayakkara, M. Challacombe, P.M.W. Gill, B. Johnson, W. Chen, M.W. Wong, C. Gonzalez, J.A. Pople, Gaussian 03, Revision C.02, Gaussian, Inc., Wallingford, CT, 2004.
[21] R. Dennington II, T. Keith, J. Millam, K. Eppinnett, W.L. Hovell, R. Gilliland, GaussView, Version 3.0, Semichem, Inc., Shawnee Mission, KS, USA, 2003.
[22] S. Grabowski, Ann. Rep. Prog. Chem., Sect. C 102 (2006) 131.
[23] P.G. Wenthold, R.R. Squires, J. Phys. Chem. 99 (1995) 2002.
[24] C. Blondel, C. Delsart, F. Goldfarb, J. Phys. B. At. Mol. Opt. Phys. 34 (2001) 281.
[25] S.T. Graul, M.E. S., R.R. Squires, Int. J. Mass Spectrom. Ion Process. 96 (1990) 181.
[26] J. Demaison, L. Margules, J.E. Boggs, Chem. Phys. 260 (2000) 65.
[27] I. Koppel, R. Pikver, A. Sugis, E. Suurmaa, E. Lippmaa, Org. React. 18 (1981) 3.